Impact of Slots on the Aerodynamic Performance of the Variable Inlet Guide Vane Cascade of a Centrifugal Compressor

J. Xin[†], X. Liu, L. Zhao, H. Wu, Z. Tian and H. Lu

School of Naval Architecture and Ocean Engineering, Dalian Maritime University, Dalian, China

†*Corresponding Author Email: xinjc@dlmu.edu.cn*

ABSTRACT

This study reconstructed the flow field of a symmetrical variable inlet guide vane in a centrifugal compressor through the passive control method of vane slots. Based on the high-fidelity numerical simulation model verified by experiments, the influence of different slot forms on the flow field was investigated, and the passive control mechanism was revealed. The results demonstrated that the vane slot method can effectively suppress the suction surface separation and broaden the range of low-loss incidence angles. Overall, the 50_30 slotted vane achieves the best flow field control, with a 65.6% reduction in the total pressure loss coefficient and a 2.3° reduction in the deviation angle, respectively, at a 25° incidence angle. The linear characteristics of the pre-swirl grade variation curve with variable inlet guide vane incidence angles are also improved. Furthermore, changing the slot outlet angle has the most significant influence on the aerodynamic performance as it changes the throat width of the location, thereby affecting the flow rate and momentum of the jet. Finally, the impact of the velocity varies in the first self-similarity region on the slotted vane. The results indicate that, in contrast to the baseline vane, the suppression effect of the slot jet on the flow separation improves with the inlet velocity, whereas the deviation angle of the slotted vane declines with the inlet velocity. Meanwhile, the higher the incoming flow velocity, the better the slotted jet can inhibition of flow separation.

Keywords: VIGV; Slot; Aerodynamic performance; Compressor; Pre-swirl.

NOMENCLATURE

c	chord length	α	stagger angle
H	cascade height	δ	maximum thickness of cascade
β	flow angle	α_1	slot inlet angle
P_{t1}	inlet total pressure	α_2	slot outlet angle
p_1	static pressure of inlet	L_1	length of slot inlet from the leading edge
Q	vortex identification criterion	L_2	distance of slot outlet from the leading edge
t	pitch length	d_1	width of slot inlet
Cpt	total pressure loss coefficient	d_2	width of slot outlet
i	incidence angle of vane	Re	Reynolds number
$\triangle\beta$	deviation angle	q	relative quantity of flow
τ	wall shear of the vane	ε	width of the slot's throat
P_{t1}	total pressure at the inlet	P_{t2}	total local pressure
P_1	static pressure at the inlet	P_t'	$P_t/ P_{t\,max}$
h	y/H	u_i, u_j	velocities in $x_i,\ x_j$ directions
x_i, x_j	Cartesian coordinates		

1. INTRODUCTION

Centrifugal compressors have been widely used to compress gas since the end of the 19th century (Krain 2005). Compressors have an essential role in many fields such as gasoline, chemicals, refrigeration, fuel cells, and storage (Guo *et al*. 2021, Zhang *et al*. 2020). Because centrifugal compressors have a low cost with higher single-stage pressure ratios, they are still widely used in the aviation field for small aircraft engines, particularly for helicopters and auxiliary power units for all types of aircraft (Agney

et al. 2018, Krain 2005). A variable inlet guide vane (VIGV) was first applied to adjust centrifugal compressor operation in the 1950s. Previous studies (Rodgers *et al.* 1991; Whitfield and Abdullah 1998) proved that when the VIGV is set to a negative pre-whirl, the compressor operating point moves to the head with a significant flow rate and power; otherwise, it moves to a low flow rate and power (Whitfield and Abdullah 1998). When the stagger angle is not 90°, the VIGV can increase the margin of stable operation of the compressor while also producing additional profile loss and throttle loss.

Various blade-profile designs have been studied to reduce the loss of VIGVs. Initially, the VIGV adopted a flat plate. When the stagger angle of the VIGV was approximately 60°, the strength of the separation bubble on the suction surface of the vane was intensified, which worsened the flow field and increased the loss of the guide vane system (Coppinger and Swain 2000). Different profiles were applied to decrease the total pressure loss coefficient (Cpt) of the VIGV. Zhang *et al.* (2009) improved the flat-plate guide vane and proposed a double-straight vane. Sanz *et al.* (1985) designed the middle arc of the blade profile as an S-type, and the results indicated that the global total pressure loss caused by the guide vane was less than 17%. Subsequently, a tandem vane was proposed. Mohseni *et al.* (2010) calculated a variable-angle series vane with fixed guide blades and rotating tail blades, which significantly decreased loss. Frank *et al.* (2021a; 2021b) studied a separation blade that can rotate both at the front and back; it exhibited a good performance even at large incidence angles when the loss of a variable inlet guide vanes system was analyzed.

Passive control involves redistributing the energy in the system and injecting part of it into the unstable region to improve the dynamic characteristics of the unstable region and the stability of the system. Existing passive flow control methods primarily include vortex generators, non-smooth solid surfaces, and slotting. Slotted blade technology is a passive control method that has been widely used in flow-field control. The main concept is to guide the fluid on the pressure surface of a blade to the suction surface through a slot, blow away the low-energy fluid around the suction surface, and weaken or suppress the flow separation. Compared with other flow control methods (Zhang *et al.* 2017; Wang 2022), its structure is simple and easy to implement. Zhou *et al.* (2008) studied the influence of the slot incident and turning angles on the flow field of an axial compressor blade. Liu *et al.* (2016) developed a slot that can decrease the number of blades to improve the thrust-to-weight ratio and avoid large separation caused by the high loading of the blades. Hu *et al.* (2018a,c) experimentally studied the influence of a novel arc slot on the flow field of a high-pressure compressor and reduced the total pressure loss by 21.9%. Tang *et al.* (2018, 2019) conducted a comparative study of full-span and ended slotted blades and observed that the loss of the end slotted blade is lower than that of the full-span slotted blade under most incidence angles. Sun *et al.* (2021) utilized multi-parameter and multi-objective

optimization of the slot to obtain the minimum total pressure loss in the cascade. Hu *et al.* (2019) observed that slots on a single-stage compressor motor blade and the static blade can inhibit the flow separation of the compressor and improve the pressure ratio of a single-stage compressor by 1.82% and the efficiency by 0.88%. Ni *et al.* (2019b) applied slotted blade technology to wind turbines. The results indicated that when the flow incidence angle was set at 11°, the lift coefficient of the slotted blade was higher than that of the baseline blade and the drag coefficient was lower than that of the baseline blade. Slotted blade technology has also been used for gas flow control and underwater airfoil drag reduction (Xie *et al.* 2020). Finally, research has also been conducted on the combination of slotted blade technology and other flow control technologies to achieve reasonable flow control (Hu *et al.* 2018b, Wang 2021).

As mentioned earlier, most investigations have focused on enhancing aerodynamic performance by optimizing the vane profile. Few studies have been conducted on the effect of slotted vane on the aerodynamic performance of the variable inlet guide vane of a centrifugal compressor. Hence, this study employed numerical simulations and experiments to study the aerodynamic performance of a baseline and slotted vanes and investigated the influence of different slots on the aerodynamic performance of the guide vane.

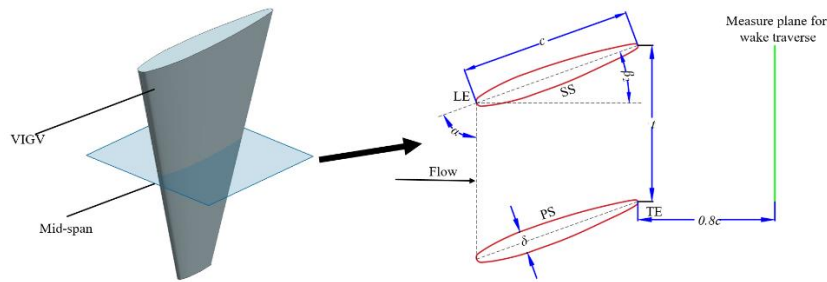## 2. GEOMETRY DESCRIPTION OF THE VANE

The VIGV was selected from a centrifugal compressor used for air separation. The guide vane operated at a wide incidence angle range of -15° to 40°. Thus, when the VIGV operated at larger incidence angles, the vane generated complex flow phenomena, such as severe suction surface (SS) separation and end-wall separation. As shown in Fig. 1, the baseline vane adopted a symmetric profile with a similar profile along the vane height direction. The midspan of the VIGV was used for the cascade study. The detailed design parameters are listed in Table 1.

Table 1 Geometrical parameters of the baseline cascade

Parameters	Values	Units
Chord length c	31.3	mm
Solidity c/t	1.08	/
Incidence angle i	-15–40	°
Flow velocity V	45	m/s
Vane height H	60	mm
Maximum thickness δ	4.1	mm

3. EXPERIMENTAL SETUP AND COMPUTATIONAL CONSIDERATIONS

In this study, we adapted the experiment and numerical methods to investigate the aerodynamic performance of the baseline and slotted guide vanes.

Fig. 1 Illustration of the base cascade.
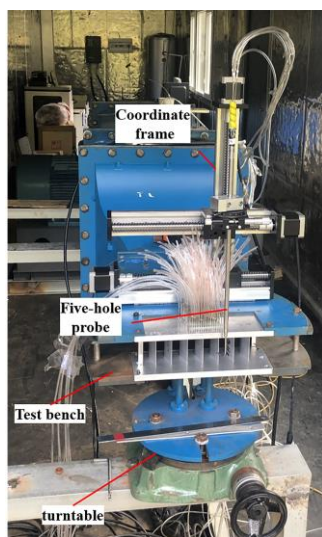
3.1 Experimental Facility

The experiments were conducted in a linear compressor cascade wind tunnel at Dalian Maritime University. Fig. 2 shows the layout of the wind tunnel and the test rig. A centrifugal fan supplied air consecutively to the test rig. The incidence angle of the cascade could be adjusted using a turntable under a wind tunnel. As shown in Fig. 2(b), because the turntable could be adjusted clockwise and counterclockwise, the stagger angle of vanes on the cascade end-wall was determined to be 70° to ensure uniformity of the flow field at the cascade inlet. In the experiment, the cascade end-wall length was 255 mm and the vane height was 60 mm. A total pressure probe was installed upstream of the wind tunnel to determine the total pressure of the incoming flow. The incoming flow incidence angle was 90° minus α, which was consistent with the traditional definition in turbomachinery. Flow velocity could be achieved by adjusting the rotational speed of the centrifugal fan motor. The baseline vane was mounted on the end-wall without any gaps to ensure air impermeability of the cascade. The coordinate frame, in which the five-hole probe was installed, was controlled using two stepper motors that could realize automatic movement in the plane.
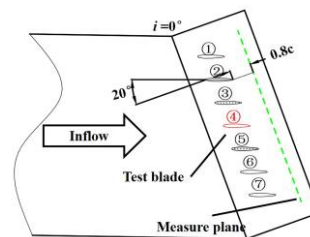
3.2 Experimental Measurement

With the movement of the coordinate frame, the five-hole probe measured the aerodynamic parameters at a plane $0.8c$ (c is the chord length) to the vane trailing edge. The diameter of the probe was 2 mm, which occupied less than 0.05% of the entire outflow plane area. Based on the vane chord, the Reynolds (Re) number in this experiment was up to 7.92×10^4. To measure the vane surface static pressure, eight static probes were placed on the vane pressure and suction surfaces. This experiment had 480 measuring points on the measuring plane with the entire vane height range at a 25° incidence angle to verify the symmetry of the flow field, and the measurement results are shown in Fig. 6. Because the cascade flow field was symmetrically distributed along with the vane height, the height of the measuring plane in other operational conditions was only 50% of the vane height, and each scenario had 264 measuring points. The pressure was measured using the digital pressure scanning valve system DSA3217 and PC software to automatically record the detected pressure signal. The sampling frequency of the scanning valve system was 5 frames per second, and 20 frames were sampled at each point with their average value output.
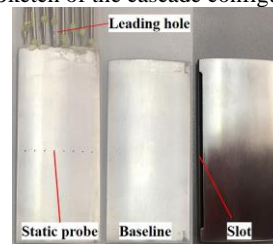
When measuring the baseline vane, the fourth vane was set as the test vane, and the static probes were processed at 50% of the height of the third and fifth vane. To ensure test periodicity, three baseline vanes at the middle positions of the cascade plate were replaced with slotted vanes (50_30), and the test method was the same as that for the baseline vane.

(a) Wind tunnel

(b) Sketch of the cascade configuration

(c) Slotted vane

Fig. 2. Wind tunnel and test rig.

3.3 Grid and Numerical Simulation Settings

The software AutoGrid5 was used to generate the baseline cascade grids, and IGG was used to generate the slot grid; both adopt structured grids. The extension of the slot in the main fluid was encrypted by considering the correct and effective data transmission between the slot and main fluids. The inlet of the computational domain was 1.5c to the leading edge of the vane, and the outlet was 2c to the trailing edge (Fig. 3). To ensure the validity of data transmission between the slot and the main flow area, the grid of the main flow area near the inlet and outlet of the slot is redivided. For all grids, the cell width at the wall was set to 0.008 mm to yield an average value of y+ < 1, which satisfied the turbulence model. The minimum orthogonality angle of all grids was larger than 17°. CFX was used to perform the simulation procedure.
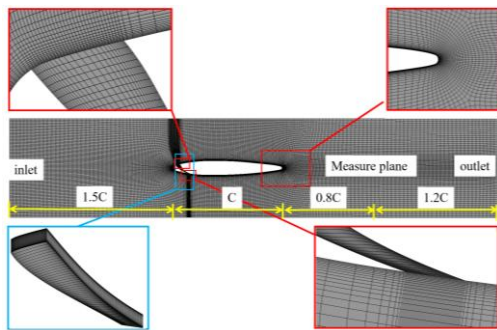

Fig. 3 Computational grid for the slotted vane.

The calculations were performed in a single passage with translational periodicity. The boundary conditions were as follows: The inflow velocity and total temperature were 45 m/s and 300 K, respectively. Six incidence angles, 0°, 10°, 20°, 25°, 30°, and 40°, were investigated. The outlet provided an area-averaged static pressure of 1 atm. The vane and end-wall were specified as adiabatic and no-slip walls, respectively. The pressure coefficient boundary layer at the inlet of the test rig was used as the boundary layer condition of the computational fluid dynamics (CFD) inlet (Fig. 4), where EXP Data represents experimental data and FIT Data was obtained from EXP Data fitting. The boundary layer thickness was 7.2 mm. Global mean residuals of less than $1 \times 10{-}6$ were considered as the convergence criteria.

$$Cpt = P_{t1} - P_{t2} / P_{t1} - P_1 \qquad (1)$$

Grid independence was investigated to eliminate the influence of the number of grids on the calculation results. Because the VIGV must be operated in a large incidence angle region, in this grid independence study, we selected a flow velocity of 45 m/s and an incidence angle of 25°. The number of grids from 2.88×10^5 to 3.50×10^6 was divided into eight different schemes. As shown in Fig. 5, the total pressure loss coefficient (*Cpt*) at the cascade outlet was used to verify the grid independence. The results showed that when the number of grids increased to

1.48 million, the total pressure loss coefficient at the outlet remained stable. Therefore, considering the trade-off between calculation accuracy and calculation cost, 1.48 million grids were adopted in this numerical simulation, and the number of slot grids was set to 1.77×10^5.
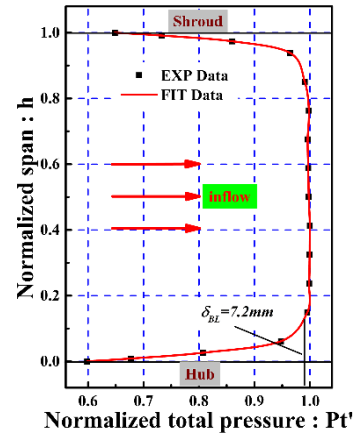

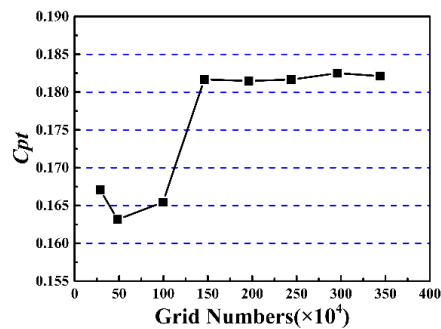**Fig. 4. Distribution of inlet pressure coefficient along the direction of the vane height.**

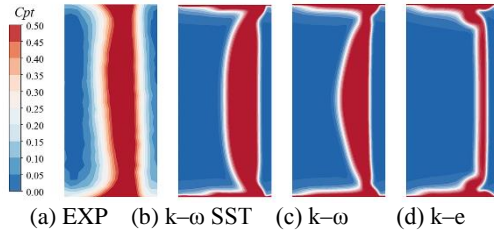**Fig. 5. Grid independency study.**

The turbulence model is a critical element in CFD. The turbulence model used in the numerical calculations was verified in this study. At an incidence angle of 25°, the baseline vane with three different turbulence models, k–e, k–ω, and k–ω shear stress transport (SST) models, were compared with the experimental results. Fig. 6 shows the contours of *Cpt* in the measurement plane. We observed that the k–ω SST model was more consistent with the experimental results. Therefore, the k–ω SST model was more accurate in capturing the flow field, and it was applied in the subsequent numerical simulation in this study. Bourgeois *et al.* (2011) and Mangani *et al.* (2012) also verified the superiority of the SST model for flow field simulation of turbomachinery.

4 SLOT SCHEME CONSIDERATION

4.1 Surface Parameters of the Baseline Vane

Fig. 7 shows the static pressure distribution at the mid-span along the chord length at different incidence angles with an incoming flow velocity of 45 m/s. The static pressure experimental results on

the vane surface at 0° incidence angle were consistent with the numerical simulation, and the other conditions were slightly different. However, the trend was the same for both datasets.

(a) EXP   (b) k–ω SST   (c) k–ω   (d) k–e

Fig. 6. *Cpt* distributions of experiments and different turbulence models on the measure plane, 25° incidence angle.

According to Fig. 7(a), when the incidence angle was smaller than 20°, the airflow separated only at the vane leading edge and attached to the suction side again at the 10% chord length until the trailing edge. Fig. 7(b) shows that when the incidence angle was larger than 25°, the airflow on the entire suction side of the vane was in a separation state. Owing to the suction side separation bubble, the suction surface pressure distribution appeared plain after the 25° incidence angle. The suction surface pressure values at different incidence angles were very close. When the incidence angle was 25°, the maximum pressure on the vane surface was primarily concentrated near the 4% chord length of the leading edge. To convert more pressure energy into kinetic energy through the slot and blow away the low-energy fluid near the suction surface, we set the inlet position of the slot at 4% of the chord length. Studies have shown that inflow control intervention before airflow separation produces the best effect (Tang *et al.* 2018). This study did not have the conditions for such an implementation and considered the loss caused by slot bend angle; thus, the slot outlet was set at 15% chord length.
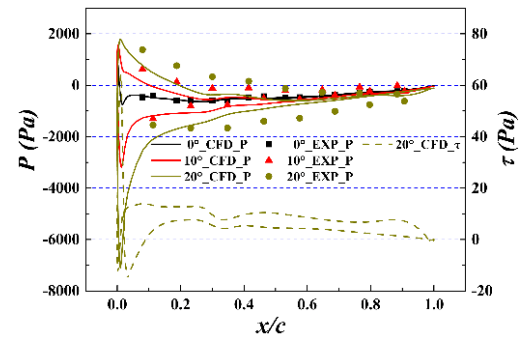
The vane separation of the suction surface was extreme when the incidence angle was greater than 25°. Therefore, the selection of the slot inlet angle primarily considered that more air flows through the slot when the incidence angle is greater than 25°. To prevent secondary flow loss caused by the slot jet, less air flows out of the slot when the incidence angle is smaller than 20°. Therefore, the inlet angle α_1 of

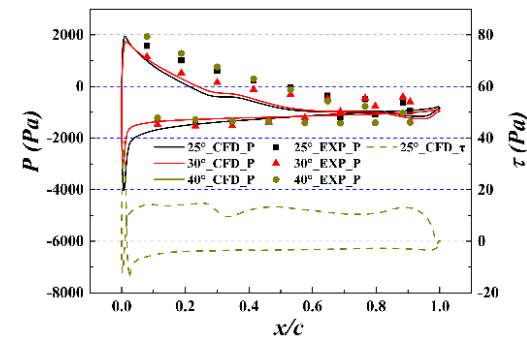the slot was set as 90° and 50° in this study.

On one hand, the position of the slot jet cannot be set before the separation point of the air flow; thus, the Coanda effect of the j*et al*one cannot effectively eliminate the separation vortex of the suction surface; on the other hand, the outlet angle of the slot is excessively large, which causes a secondary flow loss when the incidence angle is smaller than 20°; therefore, the slot outlet angle was set as 20° and 30°.

4.2 Vane Slot Configurations

Figure 8 shows the detailed structure of the slotted vane. This study maintained the slot's inlet–outlet positions and widths. The influence of different slots on the aerodynamic performance of the guide vane was studied by varying the inlet and outlet angles of the slot. The slot profile was a cubic spline curve (G2 curve) to reduce the loss caused by the slot shape.
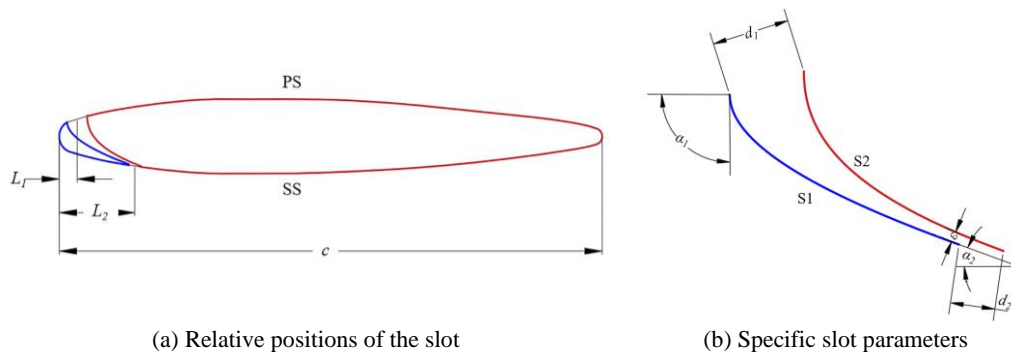

(a) 0°–20° incidence angles

(b) 25°–40° incidence angles

Fig. 7. Static pressure distributions on the vane surface with different incidence angles.

(a) Relative positions of the slot   (b) Specific slot parameters

Fig. 8. Vane slot structure.

Table 2 Geometrical parameters of the vane slot

Parameters	Values	units	Parameters	Values	units
L_1	4%c	mm	d_1	3.8%c	mm
L_2	15%c	mm	d_2	2.3%c	mm
90_20 α_1	90	°	50_20 α_1	50	°
90_20 α_2	20	°	50_20 α_2	20	°
90_30 α_1	90	°	50_30 α_1	50	°
90_30 α_2	30	°	50_30 α_2	30	°

Four differently shaped slots were studied. This study selected two inlet angles (90° and 50°) and two outlet angles (20° and 30°) and denoted them in the format of inlet angle and outlet angle. For example, 90_20 indicates a slot with an inlet angle of 90° and an outlet angle of 20° (Table 2). The slot used the pressure difference between the two vane surfaces to transfer high-momentum fluid from the pressure surface to the suction surface.
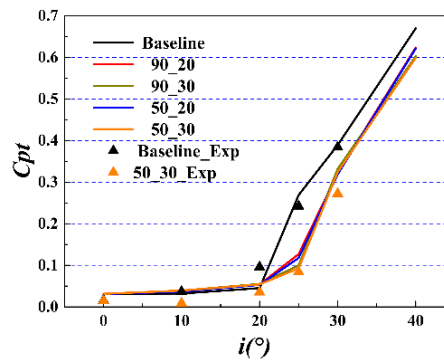
5 RESULTS AND DISCUSSION

To better present the research results, in section 5.1, the experiment and CFD results are compared, and in sections 5.2-5.5, the aerodynamic performance changes of vanes after slotting are analyzed by the CFD method.

5.1 Comparison of Experiment and CFD Results

Figure 9 shows a *Cpt* comparison of different slotted and baseline vanes to evaluate the influence of the slot jet on the aerodynamic performance. As shown in Fig. 9, when the incidence angle was from 0° to 20°, the vane's *Cpt* at the middle span increased gradually. In the range of large incidence angles (25° to 40°), the *Cpt* increased sharply. The experimental values of the baseline and slotted vanes (50_30) in the operating range agreed with the CFD values. As the guide vane was symmetrical, and the operating range of the guide vane at a negative incidence angle was -15° to 0°, the loss generated by the guide vane was also small when the guide vane operated at a negative incidence angle. Reducing the outlet loss of the guide vane at the incidence angle can improve the efficiency of the centrifugal compressor when it operates at a larger positive pre-whirl angle. Therefore, this study focused primarily on the flow control of the guide vane at a positive incidence angle.

For the four different slots, we observed that changing the inlet angle of the slot had only a slight influence on reducing the *Cpt* of the vane, but increasing the outlet angle reduced the *Cpt* of the vane to a certain extent. This was different from the results obtained for slotted vanes in an axial compressor with high loads (Tang *et al*. 2020). As the airflow separates from the vane, the initial separation position rapidly developed toward the leading edge (Fig. 7). Large separation bubbles covered the entire suction side with high strength. According to the CFD results, among the four slotted vanes, 50_30 slots had the best effect on reducing the *Cpt* when the incidence angle was large (25°–40°), and the best case was the 25° incidence angle, which reduced the *Cp*t by up to 65.6%. When the experimental incidence angle was greater than 40°, the flow field

at the inlet was slightly distorted, resulting in the experimental results being different from the simulation results. Thus, the 40° incident angle operation is not shown in Fig. 9.
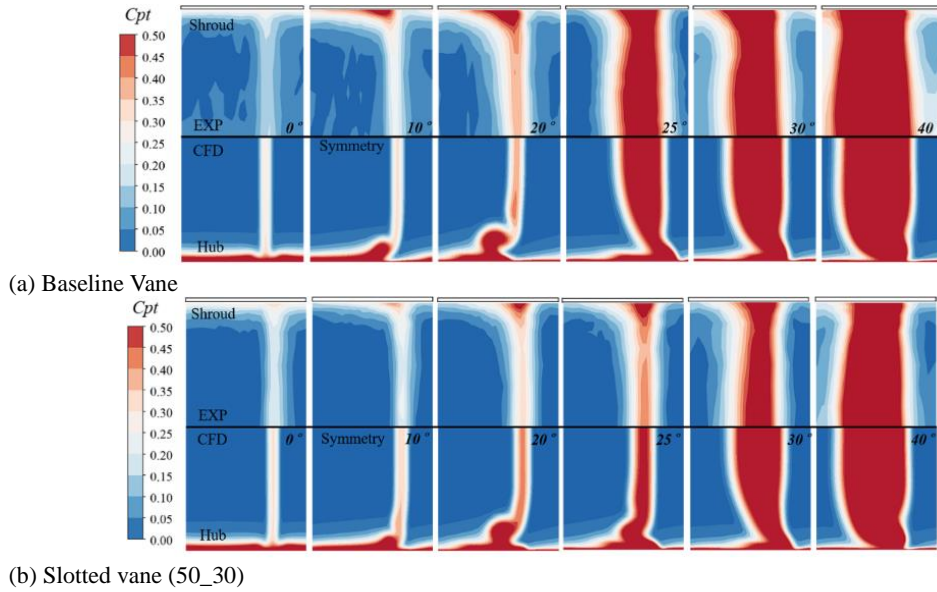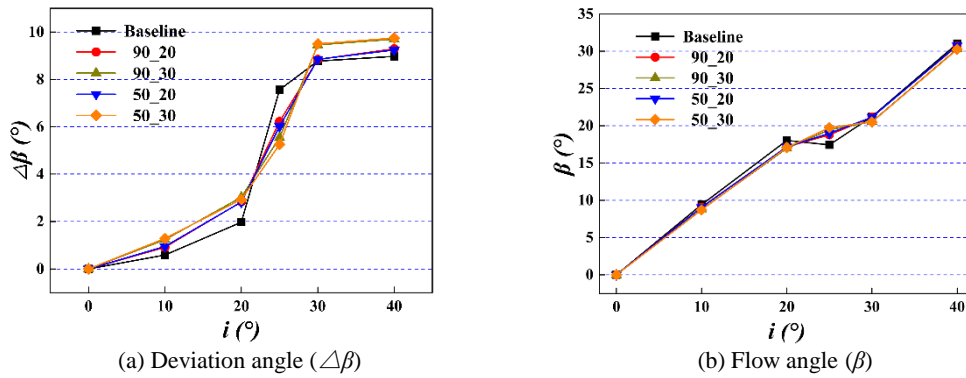

Fig. 9. Total pressure loss coefficient (*Cpt*).

The incidence angle changes the flow pressure gradient along the spanwise direction. Thus, it affects the flow separation near the vane surface and the end-wall and finally changes the range and distribution of the low-momentum fluid in the flow field. Fig. 10 shows the contours of the *Cpt* distribution at the measurement plane for six different incidence angles. The experimental results of the *Cpt* and CFD results were in good agreement at different incidence angles.

As shown in Fig. 10(a), when the airflow incidence angle was less than 20°, the high loss area at the mainstream was very small, and the high loss range increased gradually with the increase in the angle. However, as the thickness of the end-wall boundary layer increased sharply in the corner area, the loss coefficient in the corner area increased rapidly under the joint action of the end-wall secondary flow. When the incidence angle was 25°, the high loss area in the main flow area increased rapidly, and the high loss range was more extensive than the corner loss at the same incidence angle. This was because the separation bubble in the mainstream region inhibited the corner region separation.

Because the position of the fluid with high entropy and low momentum could be evaluated using *Cpt*, Fig. 10(b) shows the contours of the outlet *Cpt* of the slotted vane (50_30) at different incidence angles. At a slight incidence angle (≤20°), the slotted vanes had no evident influence on the loss coefficient of the mainstream but reduced the loss area in the corner area to a certain extent. Good results were achieved at a large incidence angle (> 20°), particularly at 25 °. In addition, the slot jet significantly reduced the high-loss area to a large extent.

(a) Baseline Vane

(b) Slotted vane (50_30)

Fig. 10 Contour comparison of *Cpt* at the cascade outlet at different incidence angles.

(a) Deviation angle ($\triangle\beta$)

(b) Flow angle (β)

Fig. 11 Flow and deviation angles of different slots.

5.2 Flow and Deviation Angles

Figure 11(a) and (b) compare the flow deviation and outlet flow angles (pre-whirl angle) between the baseline and slotted vane at different incidence angles. Fig. 11(b) shows that the outlet flow angle at an incidence angle of 25° was less than that at 20° owing to the flow separation and the sharply increased flow deviation angle. The slots effectively reduced the flow deviation angle of the cascade at an incidence angle of 25°, reduced the maximum flow deviation angle of the vane by 2.3°, and effectively improved the flow outlet angle near the incidence angle of 25°. At other incidence angles, the change in slot jet to guide the vane flow angle was less than 1°.

5.3 Cpt and Streamline Distribution of the S1 Stream Surface

Figure 12 shows the streamline distribution and *Cpt* distribution contours of the S1 stream surface at 50% vane height. Fig. 12 (a) and (c) show the airflow underwent separation from the leading edge at incidence angles of 25° and 30°. Large vortices and high-loss areas were formed on the suction side. Fig. 12 (b) shows the flow scenario of the 50_30 slotted vane at a 25° incidence angle. As shown in the figure,

the jet flow in the slot inhibited the separation of airflow to a large extent such that the airflow could reattach to the suction surface of the guide vane, and it also significantly reduced the area of the high loss. Fig. 12 (d) shows that although the slot jet did not cause the flow of the vane reattach at a 30° incidence angle, it reduced the size of the vortex and the high-loss area to an extent.
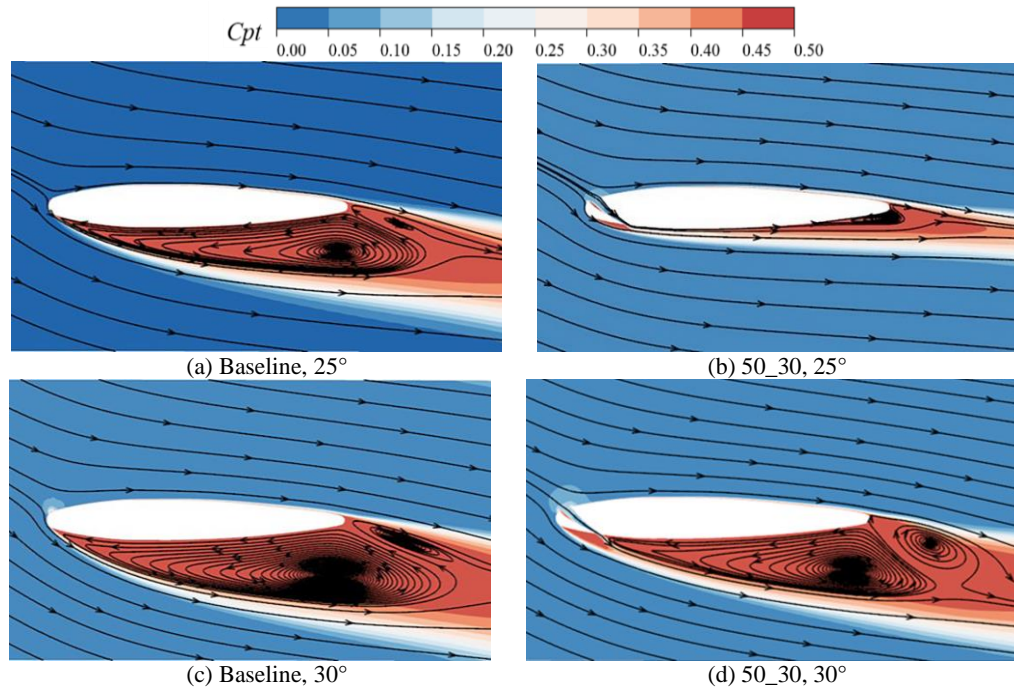
5.4 Q criterion

The Q criterion, proposed by Hunt *et al.* (1988), is widely used t identify the vortex structures in incompressible fluids. The position and development process of vortex structure in the cascade passage can be more intuitively understood by observing the Q iso-surface map, which is defined as:

$$Q = (\Omega_{ij}\Omega_{ij} - S_{ij}S_{ij}) / 2 \qquad (2)$$

$$\Omega_{ij} = (\partial u_i / \partial x_j - \partial u_j / \partial x_i) / 2 \qquad (3)$$

$$S_{ij} = (\partial u_i / \partial x_j + \partial u_j / \partial x_i) / 2 \qquad (4)$$

where Ω_{ij} is the vorticity tensor, S_{ij} is the shear strain tensor, u_i and u_j are the velocities in x_i and x_j directions, respectively, and x_i and x_j are the Cartesian coordinates.

Fig. 12 Comparisons of the *Cpt* and stream surface at the 50% span height.

In an actual annular cascade, separation already occurs near the shroud and hub at a 10° incidence angle. To analyze the influence of slotted vanes on the flow near the end-wall at a slight incidence angle more intuitively, Fig. 13 presents the vorticity diagram based on Q=0.001 and the contour of *Cpt* on the measurement plane under an incidence angle of 10°. The high-loss area in the figure matched the vorticity diagram well. As shown in the figure of the baseline cascade, a horseshoe vortex (HV) was formed when the airflow flowed through the leading edge of the vane, and the HV of the suction surface (HSV)disappeared quickly during the downstream development process. The volume of the corner vortex (CV) structure is small and close to the suction surface at a small incidence angle, so the jet had little influence on it. The passage vortices (PVs) induced by the transverse secondary flows on the pressure and suction surfaces disappeared soon because of viscous dissipation. Because the PV and HSV dissipated quickly, the slot jet had minimal effect on them, but it significantly impacted the wall concentrated shedding vortex (CSV). The CSV height of the baseline cascade accounted for 10.3% of the vane height. Compared with the baseline and the four types of slotted vanes, the jet flow at the outlet of four types of slotted vanes weakened the CSV to 7.8%, 6.1%, 7.3%, and 5.8%, respectively, to reduce the total pressure loss near the end-wall at the cascade. The effect of the 50_30 slotted vane was the most significant.

5.5 Momentum Coefficient of the Slot

Figure 14 shows the curves of the momentum coefficients of the four slots when the guide vanes operated at a positive incidence angle, defined as:

$$\zeta = (\rho_s A_s cos(\theta)V_s^2 / \rho_i A_i V_i^2) \times 100 \qquad (5)$$

where A is the area, ρ is the flow density, θ is the angle between the arc in the slot and the guide vane, and V is the average flow velocity. The subscript S indicates the outlet position of the slot, and i indicates the inlet position of the computing domain. The momentum coefficient of each slot increased with an increase in the angle because a stronger air separation requires more high-energy fluid to blow the low-energy fluid. We observed that because the outlet angle of the slot changed the slot throat width, the jet momentum coefficient of the slot with a 30° outlet angle was more significant than that with a 20° outlet angle. Reducing the inlet angle can increase the slot momentum coefficient. Combined with Fig. 9, we observed that the larger the momentum coefficient, the better the jet effect of the slot. In addition, compared with the jet angle, the jet momentum had the most significant influence on the flow field of the guide vane.

5.6 Study on the Aerodynamic Performance of Incoming Flow Velocity

Fig. 15 compares the *Cpt* and flow deviation angle at a 25° incidence angle for different vanes with the changing incoming flow velocity. The *Cpt* of the baseline cascade decreased with the incoming flow velocity, whereas the flow deviation angle increased. As the Reynolds number increased, the inlet flow became closer to turbulence, slowing down the flow separation. Hence, with an increase in the inlet flow velocity, the *Cpt* of the slotted vane decreased. However, in contrast to the baseline vane, the flow deviation angle of the slotted vanes decreased with increasing inlet flow velocity. Compared with the baseline vane, the slotted vane reduced the *Cpt* of the vane by 59.5% when the flow velocity was 30 m/s, and it achieved a reduction of 70.2 % when the flow velocity increased to 98 m/s. As the incoming flow
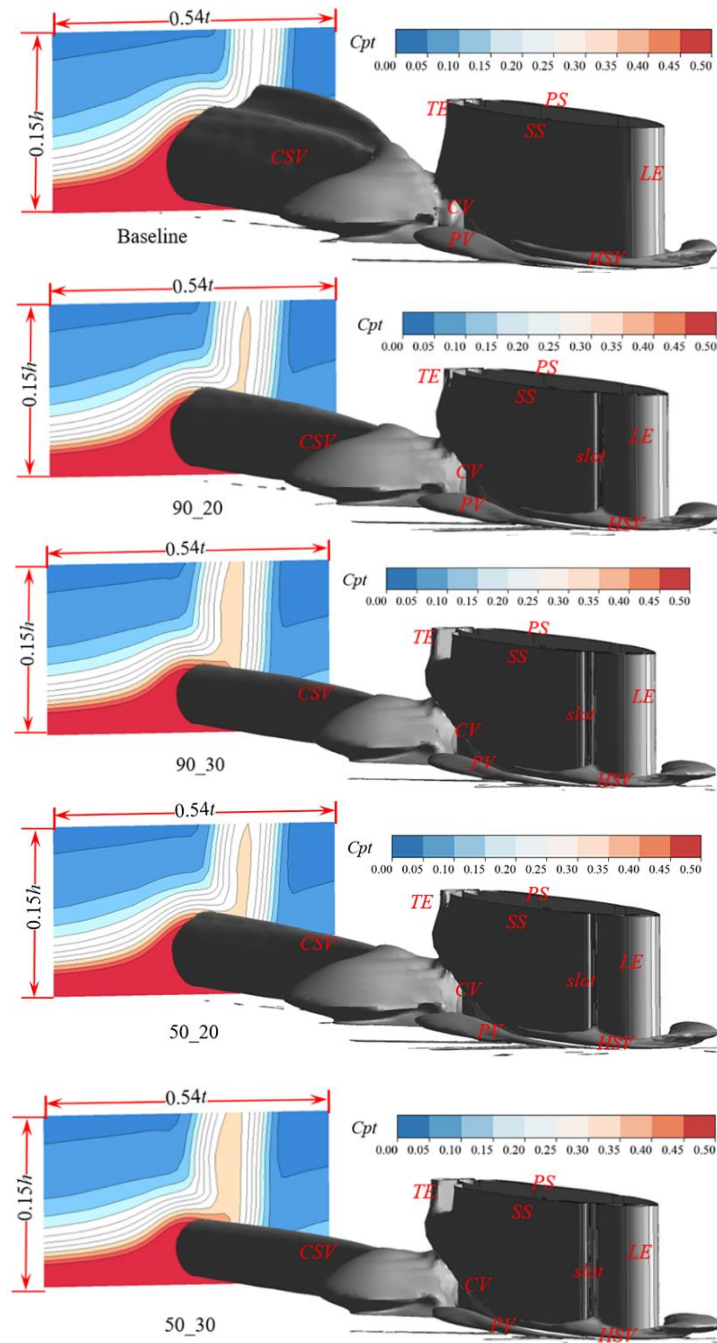
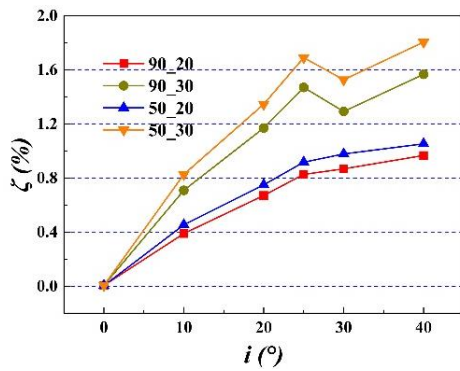**Fig. 13. Distribution of vorticity and *Cpt* of the baseline vane and four slotted vanes.**
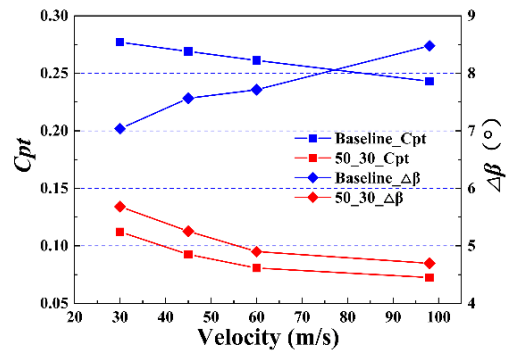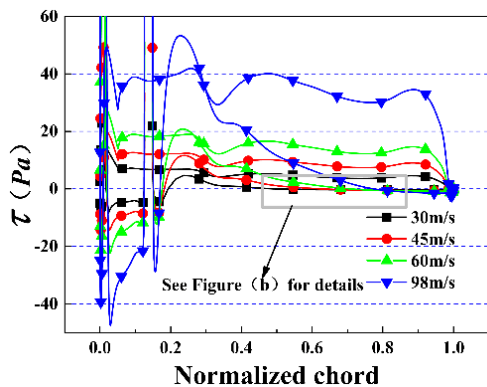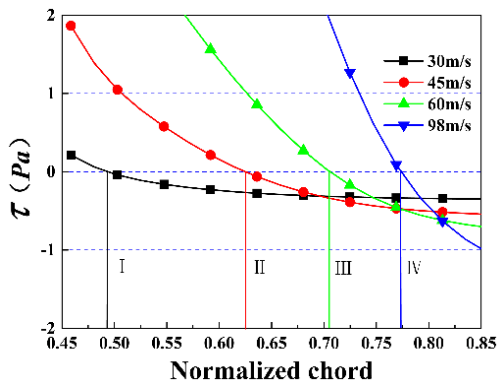

Fig. 14. Momentum coefficients.

Fig. 15. *Cpt* and deviation angle distribution at the measurement plane at 25° incidence angle under different incoming flow velocities.

velocity increased from 30 to 98 m/s, the flow deviation angle of the slotted vane decreased from 1.3° to 3.7°. This indicated that increasing the flow velocity improved the aerodynamic performance of the guide vane at a low Reynolds number.

Figure 16(a) shows the wall shear stress distribution along the axial chord length at a 25° incidence angle when the incoming flow velocity ranged from 30 to 98 m/s. The results were obtained from both surfaces of the vane. Figure 16(a) indicates that no air separation occurred on the vane pressure surface under different incoming flow velocities. The suction surface of the vane was separated at the middle chord. Fig. 16(b) shows that when the incoming flow velocity was 30 m/s, the flow of slotted vanes separated at the 49% chord length, whereas the separation positions at 45, 60, and 98 m/s were 62.5%, 70.5%, and 77% chord lengths, respectively. Therefore, with the increase in flow velocity, the effect of slotting became better.

(a) Distribution of surface shear stress over the entire vane

(b) Detailed view of suction surface

Fig. 16. Surface shear stress distribution under different flow velocities at a 25° incidence angle.

6. CONCLUSION

The influence of a symmetrical variable inlet guide vane with a slot on the aerodynamic performance of a centrifugal compressor was studied. The primary control mechanism of the slot was analyzed through experimental measurements and CFD results. According to the above analysis, the conclusions are

as follows:

1) At a high incidence angle (25°–40°), when the inlet flow velocity of the guide vane is 45 m/s, the *Cpt* at the cascade outlet can be reduced by about 65.6% at the maximum. At small incidence angles (0°–20°), the volume of the end-wall CSV can be reduced by the jet flow, and the maximum CSV height can be reduced by nearly half.

2) Because 25° is the critical incidence angle, the airflow is separated on the entire suction surface of the guide vane, resulting in a sudden increase in the deviation angle, which affects the monotonicity of the pre-swirl curve with the change in the incidence angle. The slotted jet reduces the deviation angle to a maximum of 2.5°, thereby optimizing the pre-swirl performance of the guide vane.

3) We observed that changing the inlet angle of the slot has minimal influence on the flow field, whereas changing the outlet angle can significantly influence the flow field. Combined with the momentum coefficient of the slot, the jet effect of the slot can be improved by increasing the flow through the slot under the same conditions.

4) As the incoming flow velocity increases in the self-similarity zone, the *Cpt* and deviation angle of both the baseline and the slotted vane decrease. The results showed that when the flow velocity increases, the flow field control effect of the vane slot improves.

REFERENCE

Agney, A., S. Singh and G. Srinivas (2018). Structural and fluid flow analysis of subsonic aircraft jet engine centrifugal compressor. *Materials Today: Proceedings* 5(9), 19507-19516.

Bourgeois, J. A., R. J. Martinuzzi, E. Savory, C. Zhang and D. A. Roberts (2011). Assessment of turbulence model predictions for an aero-engine centrifugal compressor. *Journal of Turbomachinery* 133(1), 011025.

Coppinger, M. and E. Swain (2000). Performance prediction of an industrial centrifugal compressor inlet guide vane system. *Proceedings of the Institution of Mechanical Engineers, Part A: Journal of Power and Energy* 214(2), 153-164.

Frank, R. G., C. Wacker and R. Niehuis (2021a). Loss Characterization of a Conventional Variable Inlet Guide Vane. *International Journal of Turbomachinery, Propulsion* 6(3), 30.

Frank, R. G., C. Wacker and R. J. J. O. T. Niehuis (2021b). Loss Characterization of Advanced VIGV Configurations With Adjustable Blade Geometry. *Journal of Turbomachinery* 144(3), 031012.

Guo, W., Z. Zuo, J. Sun, H. Hou, Q. Liang and H. J. H. Chen (2021). Experimental investigation on off-design performance and adjustment strategies of the centrifugal compressor in compressed air energy storage system. *Journal of Energy Storage* 38, 102515.

Hu, J., R. Wang, L. Renkang, H. Chen and L. Qiushi (2018). Experimental investigation on separation control by slot jet in highly loaded compressor cascade. *Proceedings of the Institution of Mechanical Engineers, Part G: Journal of Aerospace Engineering* 232(9), 1704-1714.

Hu, J., R. Wang and D. Huang (2018b). Flow control mechanisms of a combined approach using blade slot and vortex generator in compressor cascade. *Aerospace Science & Technology* 78, 320-331.

Hu, J., R. Wang, P. Wu and C. He (2018c). Separation Control by Slot Jet in a Critically Loaded Compressor Cascade. *International Journal of Turbo & Jet-Engines* 35(3), 229-239.

Hu, J., R. Wang and D. Huang (2019). Improvements of performance and stability of a single-stage transonic axial compressor using a combined flow control approach. *Aerospace Science & Technology* 86, 283-295.

Hunt, J. C., A. A. Wray and P. Moin (1988). Eddies, streams, and convergence zones in turbulent flows. *Studying Turbulence Using Numerical Simulation Databases, 2. Proceedings of the Summer Program.*

Krain, H. (2005). Review of centrifugal compressor's application and development. *Journal of Turbomachinery* 127(1), 25-34.

Liu, Y., J. Sun, Y. Tang and L. Lu (2016). Effect of slot at blade root on compressor cascade performance under different aerodynamic parameters. *Applied Sciences* 6(12), 421.

Mangani, L., E. Casartelli and S. Mauri (2012). Assessment of various turbulence models in a high pressure ratio centrifugal compressor with an object oriented CFD code. *Journal of Turbomachinery* 134(6), 061033.

Mohseni, A., E. Goldhahn, R. A. Van den Braembussche and J. R. Seume (2010). Novel IGV Designs for Centrifugal Compressors and Their Interaction With the Impeller. *Paper presented at the ASME Turbo Expo 2010: Power for Land, Sea, and Air.*

Ni, Z., M. Dhanak and T. C. Su (2019). Performance of a slotted hydrofoil operating close to a free surface over a range of angles of attack. *Ocean Engineering* 188, 106296.

Ni, Z., M. Dhanak, T. C. Su and I. Aerodynamics (2019). Improved performance of a slotted blade using a novel slot design. *Journal of Wind Engineering* 189, 34-44.

Rodgers, C. (1991). Centrifugal Compressor Inlet Guide Vanes for Increased Surge Margin. *Journal of Turbomachinery* 113(4), 696-702.

Sanz, J. M., E. R. McFarland, N. L. Sanger, T. F. Gelder and R. H. Cavicchi (1985). Design and Performance of a Fixed, Nonaccelerating Guide Vane Cascade That Operates Over an Inlet Flow Angle Range of 60 Deg. *Journal of Engineering for Gas Turbines and Power* 107(2), 477-484.

Sun, J., X. Ottavy, Y. Liu and L. Lu (2021). Corner separation control by optimizing blade end slots in a linear compressor cascade. *Aerospace Science & Technology* 114, 106737.

Tang, Y., Y. Liu and L. Lu (2019) Evaluation of Compressor Blading With Blade End Slots and Full-Span Slots in a Highly Loaded Compressor Cascade. *Journal of Turbomachinery* 141, (121002)121001-121010.

Tang, Y., Y. Liu and L. Lu (2018). Solidity effect on corner separation and its control in a high-speed low aspect ratio compressor cascade. *International Journal of Mechanical Sciences* 142, 304-321.

Tang, Y., Y. Liu and L. Lu, H. Lu and M. J. A. J. Wang (2020). Passive separation control with blade-end slots in a highly loaded compressor cascade. *AIAA Journal* 58(1), 85-97.

Wang. L., C. Wang, S. Wang, S. Qin, G. Sun, B. You and Y. Zhong (2022). A boundary surrogate model for micro/nano grooved surface structure applied in turbulence flow control over airfoil, *Chinese Journal of Aeronautics* 35(2), 62-73.

Wang, H., X. Mao, B. Liu and Y. Qingv (2021). Combined flow control with full-span slot and end-wall boundary layer suction in a large-camber compressor cascade. *Aerospace Science & Technology* 119, 107121.

Whitfield, A. and A. Abdullah (1998). The performance of a centrifugal compressor with high inlet prewhirl. *Journal of Turbomachinery* 120, 487-493.

Xie, X., S. Chang, C. Wang and C. Guo (2020). Numerical simulation of hydrodynamic performance of hydrofoil with inner groove. *Chinese Journal of Ship Research* 15(4), 127-134.

Zhang, H. , S. Chen, Q. Meng and S. Wang (2017).

Flow separation control using unsteady pulsed suction through endwall bleeding holes in a highly loaded compressor cascade. *Aerospace Science and Technology* 72(JAN.), 455-464.

Zhang, Y., D. Qi and Y. Mao (2009). Experimental investigation and improvement of the inlet guide vane with plate vane in a centrifugal fan. *Proceedings of the Institution of Mechanical Engineers, Part A: Journal of Power and Energy* 223(4), 401-413.

Zhang, Y., S. Xu and Y. Wan (2020). Performance improvement of centrifugal compressors for fuel cell vehicles using the aerodynamic optimization and data mining methods. *International Journal of Hydrogen Energy,* 45(19), 11276-11286.

Zhou, M., W. R., Z. Cao and X. Zhang (2008). Research on effect of slot inlet angle and turning angle on the flow field characteristic of cascade. *Journal of Aerospace Power* 23(1), 125-129.